Ahmer Mehmood, Muhammad Saleem Iqbal* and Irfan Mustafa

Cooling of Moving Wavy Surface through MHD Nanofluid

DOI 10.1515/zna-2016-0044
Received February 4, 2016; accepted April 17, 2016; previously published online May 11, 2016

Abstract: Heat transfer analysis has been carried out in the Magnetohydrodynamic (MHD) boundary layer formed near the wavy rough plate moving in *x*-direction. Due to the presence of metallic nanoparticle in the fluid and enhanced surface area of the plate as a consequence of surface texture, an increase in heat transfer rates is expected. However, the calculation of these enhanced rates of heat transfer is not straightforward because the convection phenomena become more complicated due to the motion of nanoparticle in the base fluid and also the waviness of the plate surface. The contribution of nanoparticle toward convective heat transfer is manifold which requires a suitable model in order to capture the correct physics. Famous Tiwari and Das model has been utilised in the current study. Percent increase in the rate of heat transfer is calculated for the nanoparticle of different metals, such as MWCNT, SWCNT, Al_2O_3, TiO_2 and Ag. Appreciable increase in the rate of heat transfer is observed, which is 24 % at the most for Al_2O_3 nanoparticle. The effect of applied magnetic field on the velocity profile, skin friction coefficient, and Nusselt number has also been presented through graphs. The concentration of the nanoparticle has been limited up to 10 %.

Keywords: Heat Transfer Enhancement; MHD; Nanofluid; Viscous Fluid; Wavy Rough Surface.

1 Introduction

Enhancement in the rate of heat transfer through irregular surface shape is a topic of fundamental importance in heat transfer processes. In practice, surface irregularities occur frequently in several manufacturing and engineering mechanisms. Body surface is sometimes intentionally roughened to enhance heat and mass transfer as a consequence of enhanced convection phenomena. Flat-plate solar collectors and flat-plate condensers in refrigerators are the examples where roughening elements are intentionally placed on a uniform body surface. The presence of roughing elements disturbs the flow which in turn expedites the convective mixing of the fluid. Consequently, the rates of heat transfer are increased.

Most conventional coolants such as water, ethylene glycol, and engine oil have low thermal properties due to which they face certain restrictions in thermal applications in comparison to solids. In particular, metals have much higher thermal conductivities as compared to liquids and therefore have high rate of heat transfer. In order to benefit from higher thermal conductivity of solid metals in convective heat transfer phenomenon, the idea of nanofluid came in reality in 1995 when Choi [1] and Choi et al. [2] pointed out the appreciable enhancement in thermal conductivity of mixture fluid formed by a base fluid and the nanoparticle. In particular, they considered suspensions of copper or aluminum nanoparticle in water and other liquids. Nanofluid is a suspension of solid nanoparticles (1–100 nm diameter) in conventional liquids such as water, oil, or ethylene glycol. This is a smart fluid, where the heat transfer capabilities can be reduced or enhanced according to the situation. These fluids enhance thermal conductivity of the base fluid enormously. The enhanced thermal behaviour of nanofluid could provide a basis for an enormous innovation for heat transfer intensification. Nanofluid is also important for the production of nanostructured materials for the engineering of complex fluids as well as for cleaning oil from surface due to their excellent wetting and spreading behaviour [3]. Advantages of nanofluid include improved heat transfer, chemical production, power generation in power plant, production of microelectronics, automotive, advanced nuclear systems, nanodrug delivery minimal clogging, microchannel cooling, and miniaturisation of the system. A significant research interest has been developed in recent years in the study of heat and mass transfer characteristics of nanofluid. There are several empirical and semi-empirical nanofluid models available in the literature. Among these, the most popular models are those proposed by Buongiorno [4, 5] and Tiwari and Das [6].

***Corresponding author: Muhammad Saleem Iqbal,** Department of Mathematics and Statistics, FBAS, International Islamic University, Islamabad 44000, Pakistan, E-mail: saleem366@yahoo.com
Ahmer Mehmood and Irfan Mustafa: Department of Mathematics and Statistics, FBAS, International Islamic University, Islamabad 44000, Pakistan

An overall survey of convective transport in nanofluid was presented by Buongiorno [4, 5] who considered a model that takes the Brownian diffusion as well as thermophoresis into account while modeling the transport equations. Nield and Kuznetsov [7–9] developed a systematic nanofluid model which also incorporates the effects of Brownian motion and thermophoresis. Different from the model proposed by Buongiorno [4, 5] and Nield and Kuznetsov [7–9], there is also a much simpler mathematical nanofluid model proposed by Tiwari and Das [6] which analyses the behaviour of nanofluid taking the solid volume fraction of nanoparticle into account.

In several practical applications, the fluids are assumed to be electrical conducting and their interaction with the applied magnetic field gives rise to the study of magnetohydrodynamics. Such situations most frequently occur in the cooling of nuclear reactor, electromagnetic casting, ship propulsion etc. Based on these interesting applications, the field of magnetohydrodynamics is an active area of research. Chamkha and Ahmed [10, 11] studied unsteady MHD heat and mass transfer in mixed-convection flow in the forward stagnation region of a rotating sphere under the influence of chemical reaction and at different wall conditions. Sheremet et al. [12] analysed magnetic field effects on the unsteady natural convection in a wavy-walled cavity filled with a nanofluid using Buongiorno's mathematical model. Mahdy and Ahmed [13] investigated soret and dufour effects on thermosolutal Marangoni boundary layer magnetohydrodynamics flow along a vertical flat plate.

Boundary layer flow on a continuous moving surface with constant speed was first studied by Sakiadis [14, 15]. Bachok et al. [16] studied the boundary layer flow of a uniformly moving nanofluid over flat plate set in motion at a constant speed. Ahmad et al. [17] discussed the Blasius and Sakiadis problems in nanofluid and observed an increase in skin friction and heat transfer coefficients. Dalir and Nourazar [18] studied the boundary layer flow of various nanofluid over a moving semi-infinite plate using HPM taking six types of nanoparticles such as copper (Cu), alumina (Al_2O_3), titania (TiO_2), copper oxide (CuO), silver (Ag), and silicon (SiO_2), and found that the Ag nanoparticle has highest values of the local skin friction coefficient. Makinde [19] analysed Sakiadis flow of nanofluid with viscous dissipation and Newtonian heating and concluded that heat transfer rate at the moving plate surface with Cu-water as the working nanofluid is higher than TiO_2-water nanofluid. The model proposed by Tiwari and Das [6] has been considered by several authors for studying the heat transfer phenomena in variety of flows. Abu-Nada [20], Oztop and Abu-Nada [21], and Abu-Nada and Oztop [22] reported heat transfer enhancement in various flow situations using Tiwari and Das model. Bachok et al. [23, 24] utilised the same model in studying flow and heat transfer phenomena over a moving boundary with and without suction/injection. Mustafa et al. [25] investigated the MHD mixed-convection stagnation point flow by considering the Tiwari and Das model. Variety of similar studies is available in literature which utilised the Tiwari and Das model to represent the working nanofluid. All these studies authenticate the validity of Tiwari and Das model in the study of convective heat and mass transfer in nanofluid boundary layer.

The gain in convective heat transfer rate as a result of increased surface area is usually not simply because of enhanced conduction between the fluid and the solid surface. Enhanced surface area also contributes toward increased vorticity transport which in turn results in increased rate of heat transfer. Keeping this fact in mind, the idea of surface roughening came in reality in order to establish enhanced vorticity transport to get heat transfer augmentation. Mathematical handling of irregular rough surface is far more difficult as compared to a regular rough surface. In this way, a smooth wavy roughness of the flat plate is quite easy to model due to its differentiable nature. However, the wavy surface contributes toward symmetry breaking, and the scaling symmetry does not leave the governing system (equations and the boundary conditions) invariant as it does for the flat plate case. Consequently, the self-similar solution does not persist anymore and the flow becomes completely non-similar. Rees and Pop [26, 27] investigated free convective boundary layer flow and heat transfer due to a wavy horizontal plate and flow and heat transfer due to a moving wavy plate. Hossain and Pop [28] studied the MHD effects on momentum and thermal boundary layer over a moving wavy plate. Ahmed et al. [29] analysed the effect of local thermal non-equilibrium on unsteady heat transfer by natural convection of a nanofluid over a vertical wavy surface. Gorla and Kumari [30] studied free convection phenomena near a vertical wavy plate in a nanofluid. Narayana et al. [31] studied double-diffusive and cross-diffusion effects on a horizontal wavy surface embedded in porous medium. Sheremet and Pop [32] using Buongiorno's mathematical model investigated natural convection in a wavy porous cavity with sinusoidal temperature distributions. Using the same mathematical model, Ghaffri et al. [33] analysed oblique stagnation point flow of a non-Newtonian nanofluid over stretching surface. Sheremet et al. [34, 35] utilising nanofluid-famous Tiwari and Das model investigated steady and unsteady natural convection phenomena in a porous wavy cavity. Javed et al. [36] discussed MHD effects on the

natural convection of Cu-water nanofluid in a triangular cavity. Elshehabey et al. [37] investigated numerically natural convection of a nanofluid in an inclined L-shaped cavity in the presence of an inclined magnetic.

In all the above mentioned studies, authors considered pure fluid for the computation of the increased rate of heat transfer due to the wavy surface. Further increase in the rate of heat transfer is expected if one considers nanofluid instead of pure fluid over a wavy plate. Being motivated by this fact, we consider flow and heat transfer characteristic of nanofluid over a moving wavy plate. Tiwari and Das [6] model has been utilised in this study and nanofluid is considered as a mixture of water and nanoparticle. Nanoparticles of five different metals such as MWCNT, SWCNT, Al_2O_3, TiO_2, and Ag are used and the increase in heat transfer rate is noted for every metal separately. Maximum increase in heat transfer rate is observed for alumina which is almost 24 % at 10 % nanoparticle concentration.

2 Mathematical Formulation

We consider a non-flat wavy sheet extended in *x*- and *y*-directions whose surface is described by the function

$$\bar{y}=\bar{S}(\bar{x})=\bar{\alpha}sin\left(\frac{\pi\bar{x}}{l}\right), \tag{1}$$

where $\bar{\alpha}$ is the fixed amplitude and l is the wave length. The wavy surface starts from the line $x=0$ in the xz-plane and is assumed to be surrounded by the ambient nanofluid. The schematic of the wavy plate and the coordinate system is shown in Figure 1.

Since the plate is symmetric about the *x*-axis, it is reasonable to investigate the convection phenomena in the domain $y \geq \bar{S}(\bar{x})$. Furthermore, the plate is identical in *z*-direction, and it is also assumed that there is no disturbance in the *z*-direction. Therefore, the flow is two dimensional in nature, and due to wavy surface of the plate, the velocity varies continuously with the variable '*x*' which makes the flow non-similar. In this way, the domain of *x* ($x \geq 0$) is of fundamental importance. The flow is assumed to be caused due to the uniform motion of the wavy plate in the positive *x*-direction. A uniform magnetic field of strength B_0 is applied along the *y*-direction. The magnetic Reynolds number is assumed to be very small so that the induced magnetic field can be ignored.

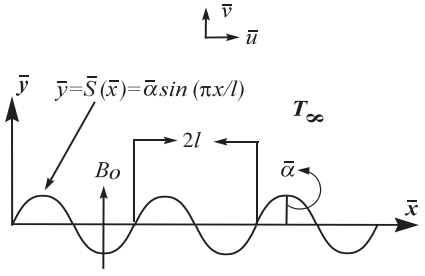

Figure 1: Physical model and coordinate system.

The study of convective transport in nanofluid requires a suitable model that can successfully capture the contribution of nanoparticle in flow and heat transfer phenomena. The aforementioned Tiwari and Das model [6] considers the improved material properties of the nanofluid. Practically, the nanoparticle contributes in convective phenomena in two ways: first by changing the material properties of the base fluid and second through their Brownian motion within the base fluid.

The ambient fluid is assumed to be the viscous nanofluid described by the Tiwari and Dass model. According to this model, the two-dimensional mass, momentum, and energy conservation laws have the form

$$\frac{\partial\bar{u}}{\partial\bar{x}}+\frac{\partial\bar{v}}{\partial\bar{y}}=0, \tag{2}$$

$$\bar{u}\frac{\partial\bar{u}}{\partial\bar{x}}+\bar{v}\frac{\partial\bar{u}}{\partial\bar{y}}=-\frac{1}{\rho_{nf}}\frac{\partial\bar{p}}{\partial\bar{x}}-\frac{\sigma_{nf}B_0^2}{\rho_{nf}}\bar{u}+\nu_{nf}\nabla^2\bar{u}, \tag{3}$$

$$\bar{u}\frac{\partial\bar{v}}{\partial\bar{x}}+\bar{v}\frac{\partial\bar{v}}{\partial\bar{y}}=-\frac{1}{\rho_{nf}}\frac{\partial\bar{p}}{\partial\bar{y}}+\nu_{nf}\nabla^2\bar{v}, \tag{4}$$

$$\bar{u}\frac{\partial T}{\partial\bar{x}}+\bar{v}\frac{\partial T}{\partial\bar{y}}=\alpha_{nf}^{*}\nabla^2 T, \tag{5}$$

where $\bar{u}$ and $\bar{v}$ are the components of velocity along the *x*- and *y*-directions, respectively, T is the temperature, $\bar{p}$ is the pressure, ρ_{nf} be the density, α_{nf}^{*} be the thermal diffusivity, σ_{nf} be the effective electric conductivity of nanofluid [37], B_0 be the strength of uniform magnetic field, T_∞ is the constant ambient temperature, and ∇^2 is the Laplacian operator. The relations for μ_{nf}, ρ_{nf}, σ_{nf}, α_{nf}^{*}, and $(\rho c_p)_{nf}$ are described as

$$\begin{aligned}
&\mu_{nf}=\frac{\mu_f}{(1-\phi)^{2.5}},\ (\rho c_p)_{nf}=(1-\phi)(\rho c_p)_f+\phi(\rho c_p)_p,\\
&\rho_{nf}=(1-\phi)\rho_f+\phi\rho_p,\\
&\alpha_{nf}^{*}=\frac{\kappa_{nf}}{(\rho c_p)_{nf}},\quad \frac{\kappa_{nf}}{\kappa_f}=\frac{(\kappa_p+2\kappa_f)-2\phi(\kappa_f-\kappa_p)}{(\kappa_p+2\kappa_f)+\phi(\kappa_f-\kappa_p)},\\
&\frac{\sigma_{nf}}{\sigma_f}=1+\frac{3((\sigma_p/\sigma_f)-1)\phi}{((\sigma_p/\sigma_f)+2)+\phi((\sigma_p/\sigma_f)-1)},
\end{aligned} \tag{6}$$

in which ϕ is the solid volume fraction of nanoparticle and ρ, (ρc_p), κ, and σ are the density, heat capacity, thermal conductivity, and electric conductivity, respectively. The subscripts, '*f*', '*p*', and '*nf*' refer to the base fluid, nanoparticle, and the nanofluid, respectively. The thermal conductivity κ_{nf} of nanofluid given in (6) was described by Maxwell Garnett [38] in 1904.

The wavy plate is assumed to be moving with uniform velocity in *x*-direction. Keeping in view the flow schematic and the coordinate system along with the assumed flow conditions, the resultant velocity along the wavy surface and along the normal to the wavy surface are $\bar{u}\bar{t}_{\bar{y}}+\bar{v}\bar{t}_{\bar{x}}$ and $\bar{u}\,\bar{t}_{\bar{y}}-\bar{v}\,\bar{t}_{\bar{x}}$, respectively. The appropriate boundary conditions for the velocity components and temperature function are described as (see for instance [28])

$$\begin{aligned}\bar{y}=\bar{S}(\bar{x})\colon\ &\bar{u}\bar{t}_{\bar{y}}-\bar{v}\bar{t}_{\bar{x}}=0,\ \bar{u}\bar{t}_{\bar{y}}+\bar{v}\bar{t}_{\bar{x}}=U,\ T=T_w \text{ for all } \bar{x}>0,\\ \bar{y}\to\infty\colon\ &\bar{u}=\bar{v}=0,\ \bar{p}=p_\infty,\ T=T_\infty \text{ for all } \bar{x}>0,\end{aligned} \tag{7a}$$

where $\hat{t}=(\hat{t}_x,\hat{t}_y)=\left(\frac{1}{\omega},\frac{\bar{S}_{\bar{x}}}{\omega}\right)$ is unit vector tangent to the wavy surface, for details the reader is referred to follow [28]. Since the boundary layer starts to develop at $x>0$, at the leading edge $\bar{x}=0$, the ambient flow conditions are assumed to be valid which are given by

$$\bar{x}=0\colon \bar{p}=p_\infty,\ T=T_\infty \text{ for all } \bar{y}\neq 0. \tag{7b}$$

In this case, the characteristic length is the wave length '*l*' and the reference velocity is the plate velocity *U*. All the lengths are non-dimensionalised by '*l*' and all the velocities are non-dimensionalised by the reference velocity *U*. Temperature difference $T_w - T_\infty$ is used to non-dimensionalise the temperature function. The surface undulations are assumed to be small such that $\alpha \ll \delta$, where δ is the boundary layer thickness. In this way, the governing equations in dimensionless form under the boundary layer assumptions read as

$$\frac{1}{d_1}f'''+\frac{1}{2}ff''-2\frac{\omega_\xi}{\omega}f'^2-\frac{Md_4\xi}{d_2}f'=\xi\left[f'\frac{\partial f'}{\partial\xi}-f''\frac{\partial f}{\partial\xi}\right], \tag{8}$$

$$\frac{d}{d_3 Pr}\theta''+\frac{1}{2}f\theta'=\xi\left[f'\frac{\partial\theta}{\partial\xi}-\theta'\frac{\partial f}{\partial\xi}\right], \tag{9}$$

where the dimensionless variables are defined as

$$\begin{aligned}&\xi=x=\frac{\bar{x}}{l},\ y=\frac{\bar{y}}{l},\ u=\frac{\bar{u}}{U},\ S=\frac{\bar{S}(\bar{x})}{l},\ v=\frac{\sqrt{Re}}{U}(\bar{v}-S_\xi\bar{u}),\ p=\frac{\bar{p}}{\rho_f U^2},\\ &\theta(\xi,\eta)=\frac{T-T_\infty}{T_w-T_\infty},\ \psi(\xi,\eta)=\sqrt{\xi}f(\xi,\eta),\ p=\frac{\bar{p}}{\rho_f U^2},\\ &\eta=\frac{(\bar{y}-\bar{S}(\xi,\eta))\sqrt{Re}}{l\omega\sqrt{\xi}}y,\ u=\frac{\partial\psi}{\partial x},\ v=-\frac{\partial\psi}{\partial y}\end{aligned} \tag{10}$$

in which variables η and f are being stretched by $\sqrt{\xi}$ in order to facilitate with numerical computations. Here, $\mathrm{Re}=Ul/\nu_f$ is a Reynolds number, $M=\sigma_f B_0^2/\rho_f U$ is the magnetic parameter, and $\mathrm{Pr}=\nu_f/\alpha_f$ is the Prandtl number. The subscript ξ denotes derivative with respect to ξ and the '' denotes differentiation with respect to η. The parameter $\omega=\sqrt{1+S_\xi^2}$ and $\omega_\xi=d\omega/d\xi$ denote the wavy contribution in the governing equations. The material parameters *d*, d_1, d_2, d_3, and d_4 are given by

$$\begin{aligned}&d=\frac{\kappa_{nf}}{\kappa_f},\ d_1=(1-\phi)^{2.5}[1-\phi+\phi(\rho_p/\rho_f)],\ \ d_2=[1-\phi\phi(\rho_p/\rho_f)],\\ &d_3=[1-\phi+\phi((\rho c_p)_p/(\rho c_p)_f)],\\ &d_4=1+\left(\frac{3((\sigma_p/\sigma_f)-1)\phi}{((\sigma_p/\sigma_f)+2)-\phi((\sigma_p/\sigma_f)-1)}\right)\end{aligned} \tag{11}$$

Following (10), the boundary conditions in dimensionless form read as

$$\begin{aligned}f(\xi,0)=0,\ \ f'(\xi,0)=\omega,\ \ \theta(\xi,0)=1,\\ f'(\xi,\infty)=0,\ \ \theta(\xi,\infty)=0.\end{aligned} \tag{12}$$

The physical quantities of interest such as the local skin friction coefficient and local Nusselt number are defined as

$$C_{fx}=\frac{\tau_w}{\rho_f U^2},\ \mathrm{Nu}_x=\frac{\bar{x}q_w}{\kappa_f(T_w-T_\infty)}, \tag{13}$$

where τ_w is the wall shear stress and q_w is the wall heat flux which are given by

$$\tau_w=\mu_{nf}(\nabla\bar{u}\cdot\hat{n})_{y=0},\ q_w=-\kappa_{nf}(\nabla T\cdot\hat{n})_{y=0}, \tag{14}$$

in which $\hat{n}=(n_x,n_y)=\left(-\frac{S_\xi}{\omega},\frac{1}{\omega}\right)$ (see [39]) is the unit normal to the wavy surface. After using (10) and (14), the skin friction coefficient and local Nusselt number [40] take the form

$$\begin{aligned}&C_f=C_{fx}\mathrm{Re}^{1/2}=\frac{x^{-3/2}}{\omega^{3/2}(1-\phi)^{2.5}}f''(\xi,0),\\ &\mathrm{Nu}=\mathrm{Nu}_x\mathrm{Re}^{-\frac{1}{2}}=-\frac{x^{\frac{1}{2}}}{\omega^{\frac{1}{2}}}\frac{\kappa_{nf}}{\kappa_f}\theta'^{(\xi,0)}.\end{aligned} \tag{15}$$

Due to non-similar nature of the solution, the mean values of the physical quantities are therefore preferred which are defined as

$$C_{f\,\mathrm{avg}} = \frac{1}{L}\int_0^{L=\xi} C_f(\xi)\,d\xi \text{ Or } C_{f\mathrm{avg}}\mathrm{Re}^{1/2}$$
$$= \frac{1}{L(1-\phi)^{2.5}}\int_0^{L=\xi} \frac{x^{-3/2}}{\omega^{3/2}} f''(\xi, 0)\,d\xi,$$
$$\mathrm{Nu}_{\mathrm{avg}} = \frac{1}{L}\int_0^{L=\xi} \mathrm{Nu}(\xi)\,d\xi \text{ Or } \mathrm{Nu}_{\mathrm{avg}}\mathrm{Re}^{-1/2}$$
$$= -\frac{1}{L}\frac{\kappa_{nf}}{\kappa_f}\int_0^{L=\xi} \frac{x^{1/2}}{\omega^{1/2}}\theta'^{(\xi, 0)}\,d\xi, \tag{16}$$

where L is the length of the wavy sheet measured along the x-coordinate. The average skin friction and average Nusselt number in (16) have been calculated numerically.

3 Numerical Solution

The governing non-similar systems (8) and (9) subject to boundary conditions (12) are solved numerically by Keller Box scheme [41–44] together with implicit finite-difference method. According to this procedure, the partial differential equations are first reduced to a system of first-order differential equations which are further expressed in finite difference form by approximating the functions and their derivatives in terms of the central difference approximation. The central difference approximations reduce the system of first-order differential equations to a system of non-linear difference equations. These equations are then linearised by the Newton's method and are solved using block tridiagonal algorithm. The grid independence of the present numerical solution has also been verified by making several runs for different step size for η and ξ variables. It is observed that the numerical solution does not change when $\Delta\eta < 0.005$ and $\Delta\xi < 0.005$. Finally, the present solution have been calculated by choosing $\Delta\eta = 0.005$ and $\Delta\xi = 0.005$. Table 1 contains a grid-independent test for the present technique.

In order to investigate the accuracy and validity of the present results, a comparison with the data available in the literature has been made. It is clear from Table 2 that the numerical values of the skin friction coefficient $C_{fx}\mathrm{Re}_x^{1/2}$ and local Nusselt number $\mathrm{Nu}_x\mathrm{Re}_x^{-1/2}$ for $\mathrm{Pr} = 0.7$, when $M = \alpha = 0.0$, are in excellent agreement with the result published by Rees and Pop [27] and Hossain et al. [28]. Another comparison of the present results for the values of $f''(\xi, 0)$ with those published by Chaim [45] is given in Table 3. Again an excellent agreement is observed which authenticates the present numerical procedure. We use the same procedure to solve (8), (9), and (12) numerically.

Table 1: Gird independence test for pure fluid ($\phi = 0.0$) when $\alpha = 0.2$, $M = 0.5$.

No. of grid points η direction With fix $\eta = 15$	No. of grid points ξ direction With fix $\xi = 2$	$-C_f$	Nu
100	10	0.60881	1.7097
300	20	0.54728	1.7150
600	50	0.51177	1.7193
1000	100	0.50023	1.7205
1500	200	0.49450	1.7212
2000	400	0.49164	1.7215
3000	400	0.49164	1.7215

Table 2: Comparison of present results with already-published data when $\mathrm{Pr} = 0.7$, $M = \alpha = 0.0$.

	Present	Rees and Pop [27]	Hossain et al. [28]
$C_{fx}\mathrm{Re}_x^{1/2}$	−0.44375	−0.4438	−0.4439
$\mathrm{Nu}_x\mathrm{Re}_x^{-1/2}$	−0.34924	−0.3492	−0.3509

Table 3: Comparison of values of $f''(\xi, 0)$ when $\mathrm{Pr} = 0.7$, $M = 0.5$, $\alpha = 0.0$.

	Present	Chaim [45]
ξ	$f''(\xi, 0)$	$f''(\xi, 0)$
0.0	−0.443748	−0.443751
0.1	−0.478389	−0.47696
0.5	−0.605687	−0.604488
1.0	−0.751703	−0.752938

4 Discussion

In most part of this section, we take $\mathrm{Pr} = 7.0$, $M = 0.5$, $\alpha = 0.2$, $\phi = 0.1$, otherwise mentioned. In graphical figures, solid lines represent the solution at $\xi = 0.5$ (crest), broken lines at $\xi = 1.0$ (node), and dotted lines at $\xi = 1.5$ (trough). It is observed that these quantities vary periodically in the direction of ξ when $\alpha \neq 0$ (wavy surface) and wavy effects become more pronounced when the values of α are increased.

Velocity graphs are plotted in Figures 2 and 3 against η for different values of M and α, respectively. Figure 2 shows that velocity decreases by increasing the magnetic field strength which in turns reduces the boundary layer thickness. This is because of the reason that the applied magnetic field generates the Lorentz force which acts as a retarding force due to which the momentum boundary layer thickness decreases. Figure 2 also depicts that the velocity is maximum at the crest and minimum at trough.

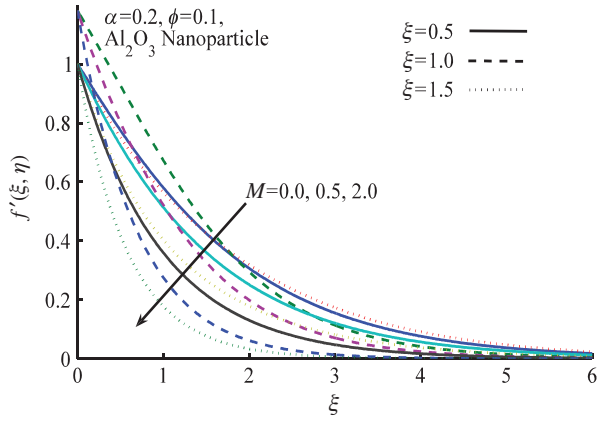

Figure 2: Effect of magnetic field on velocity profile.

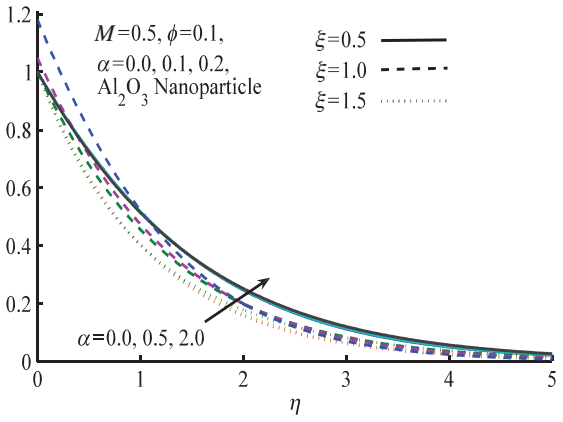

Figure 3: Effect of amplitude-to-wavelength ratio α on velocity profile.

Figure 3 highlights the impact of amplitude-to-wavelength ratio parameter α on velocity profile at crest, node, and trough locations on the wavy surface. Clearly, the velocity increases by increasing the values of α which highlights the role of surface undulation height toward enhanced convective phenomena. The velocity character at different values of ξ is the same as it was in previous graph. The effect of α on temperature profile is shown in Figure 4. It is seen that the variation in α does not bring significant change in the temperature profile; however, the temperature is observed to be minimum at crest and maximum at the node. This is because of the slow convection in the trough region as depicted in Figure 2. The effect of concentration parameter ϕ on velocity and temperature profiles is shown in Figures 5 and 6, respectively. Clearly, by increasing the concentration of nanoparticle, the velocity decreases and temperature increases. This is an obvious consequence of enhanced convection phenomena due to the presence of nanoparticle in the fluid. Local skin

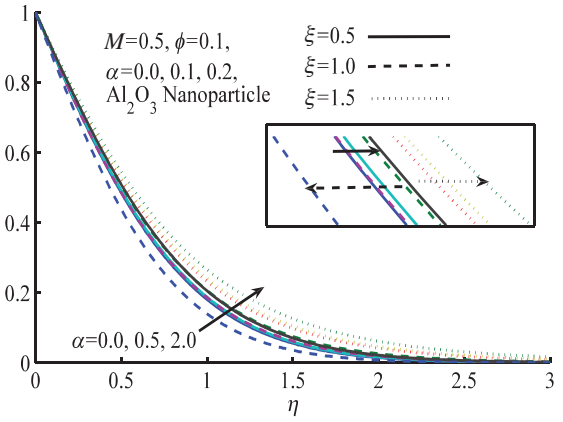

Figure 4: Temperature profile for different values of α.

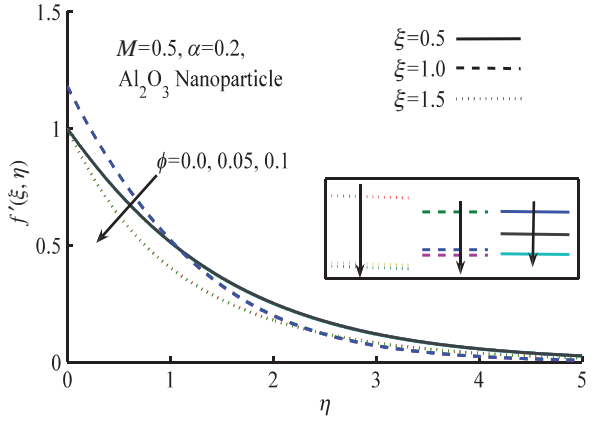

Figure 5: The effect of volume fraction parameter ϕ on velocity profile.

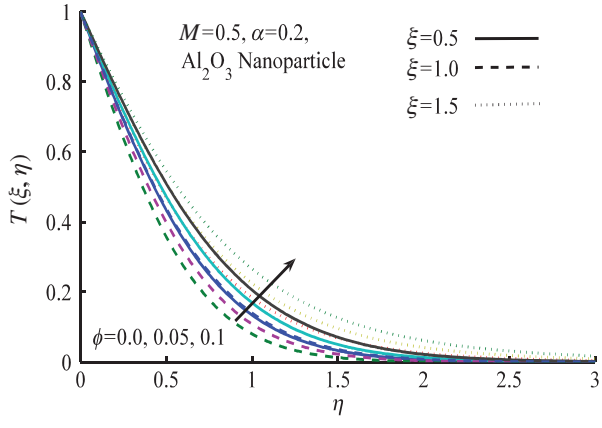

Figure 6: The effect of ϕ on temperature profile.

friction and local Nusselt number are plotted in Figures 7 and 8, respectively, for different values of α It is seen that skin friction decreases by increasing the values of α and the Nusselt number also have the same character. This

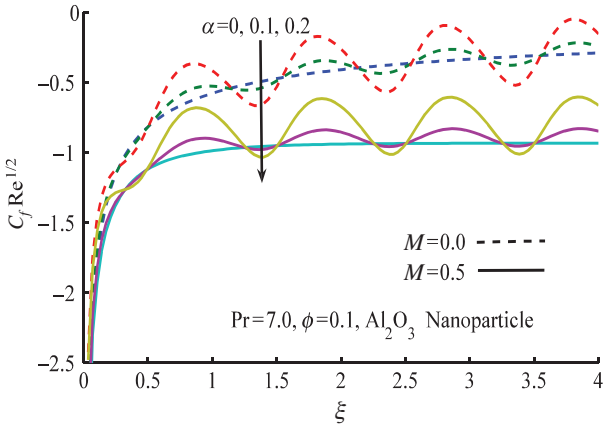

Figure 7: Skin friction plotted against ξ for different α.

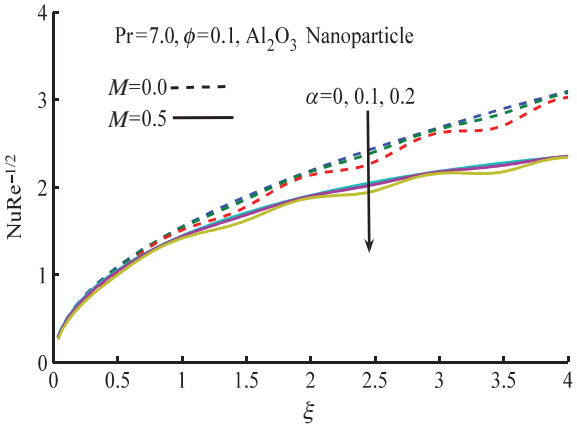

Figure 8: Nusselt number graph for different α.

fact can simply be understood from Figures 3 and 4 where the velocity and temperature increase by increasing the values of α It is seen that at crest position, the velocity is maximum, whereas at trough, it is minimum.

The current analysis has been carried out for five different types of nanoparticles such as alumina (Al_2O_3), silver (Ag), single-wall carbon nanotube (SWCNT), multiple-wall carbon nanotube (MWCNT), and titanium oxide (TiO_2). Table 4 shows the thermophysical properties of water and the five elements MWCNT, SWCNT, Al_2O_3, TiO_2 Ag. The Prandtl number of the base fluid (water) is taken as 7.0. The aim is to investigate the effect of different nanoparticle on skin friction and heat transfer on a continuous moving wavy surface in a quiescent electrically conducting fluid with a constant transverse magnetic field. To compare the skin friction and heat transfer for different nanoparticles, base liquid is considered to be water. It is worth mentioning that this study reduces the governing equations (8) and (9) to those of a viscous or regular fluid

Table 4: Thermophysical properties of base fluid and nanoparticle.

Properties	C_p(J/KgK)	ρ(Kg/m³)	κ(W/mK)	σ(S/m)
Fluid (water)	4179	997.1	0.613	0.05
Al_2O_3	765	3970	40	3.5×10^7
Ag	235	10500	429	6.3×10^7
TiO_2	686.2	4250	8.9538	0.26×10^7
SWCNT	425	2600	6600	1×10^4
MWCNT	796	1600	3000	1×10^5

when $\phi = 0$. Skin friction and Nusselt number are plotted against the solid volume fraction ϕ and wavy amplitude α for different types of nanoparticles (MWCNT, SWCNT, Al_2O_3, TiO_2, Ag) in Figures 9–12. The effect of solid volume fraction ϕ and wavy amplitude α on the local skin friction is shown in Figures 9 and 10. Clearly, the skin friction decreases by increasing ϕ and increases for increasing values of α; in both cases, the skin friction is maximum for MWCNT and minimum for Ag. The effect of solid volume fraction ϕ and wavy amplitude α on the local Nusselt number is shown in Figures 11 and 12. In both cases, Nusselt number is maximum for Al_2O_3 and minimum for SWCNT having increasing behaviour against the solid volume fraction ϕ, but opposite behaviour against wavy amplitude α. It is worth mentioning that according to (15), the Nusselt number is a product of the temperature gradient and the thermal conductivity ratio (conductivity of the nanofluid to the conductivity of the base fluid). Increasing ϕ leads to an increase in the thermal conductivity ratio which in turn increases the Nusselt number. Figure 12 depicts that the Nusselt number decreases by increasing the parameter α; this is because of the reason that the temperature increases by increasing the values of α within the boundary layer. Stream lines and isotherms are plotted in Figures 13 and 14, respectively. The wavy

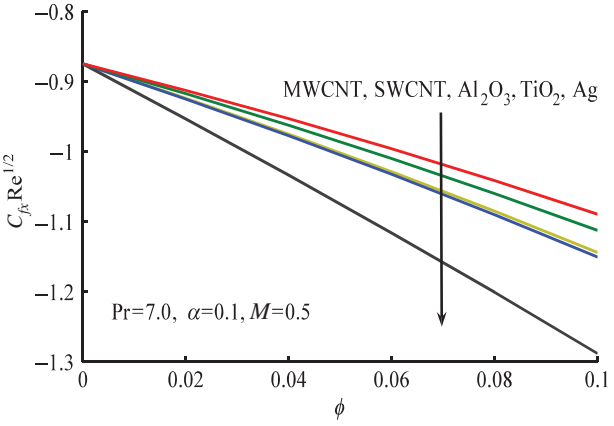

Figure 9: Skin friction plotted against ϕ for different nanoparticles.

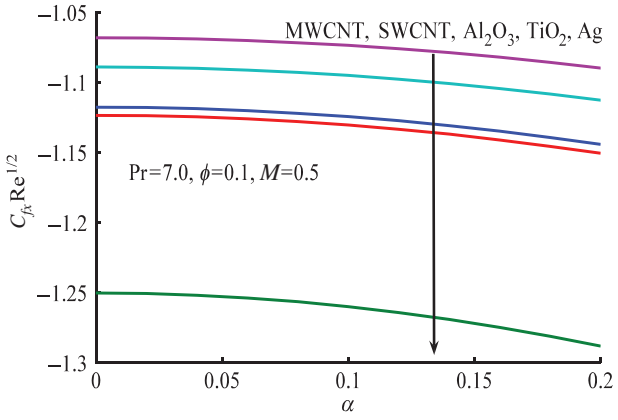

Figure 10: Skin friction behaviour for different nanoparticles against α.

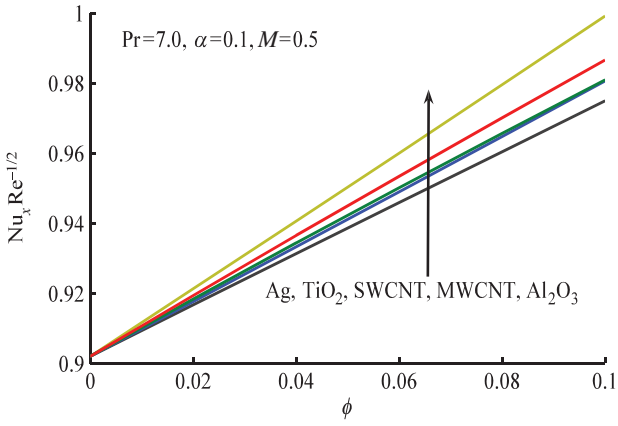

Figure 11: Nusselt number behaviour against ϕ for different nanoparticles.

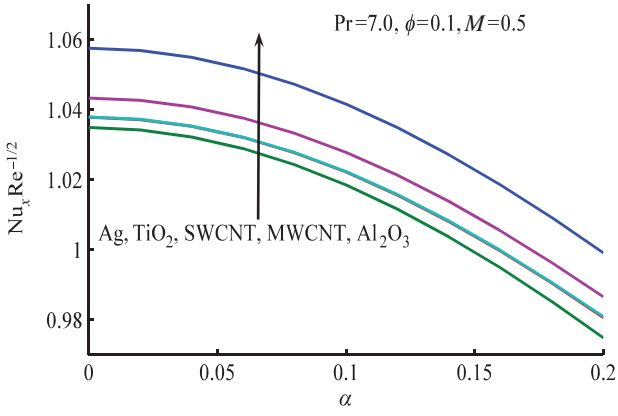

Figure 12: Nusselt number plotted against α for different nanoparticles.

pattern can easily be seen in the stream lines and isotherms graphs.

Numerical values of skin friction and rate of heat transfer for different values of α and ϕ when Pr = 7.0,

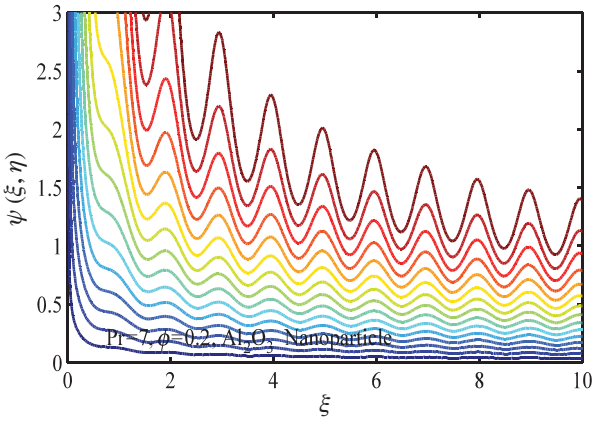

Figure 13: Stream function plotted at $\alpha = 0.2$.

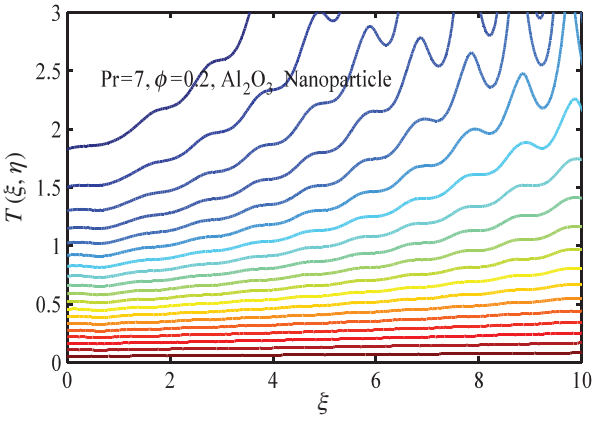

Figure 14: Isotherms plotted at $\alpha = 0.2$.

$M = 0.5$ for alumina (Al_2O_3) on the wavy surface at $x = 0.5$, $x = 1.0$, and $x = 1.5$ are presented in Table 5. It is observed that the Nusselt number decreases with the increase in α and increases with the increase in ϕ; on the other hand, opposite behaviour is seen in case of skin friction.

Percent increase in the magnitude of the skin friction and Nusselt number is calculated in Table 6 at three different locations, crest, node, and trough, on the wavy surface. It is observed that at crest, the skin friction increases by increasing the wavy amplitude at fixed concentration of nanoparticle, whereas the Nusselt number decreases. Similarly, for a fixed value of α, the skin friction increases by increasing the nanoparticle concentration. The behaviour of Nusselt number is little bit reverse as it can be seen from Table 6. The similar behaviour is followed by the skin friction and Nusselt number at the node and trough locations, however, with different numerical values. The nature of nanoparticle has fundamental role in enhancing the convective heat transfer phenomena. Table 7 shows the percent change in skin

Table 5: Values of skin friction and Nusselt number for different values of α and ϕ when Pr = 7.0, $M = 0.5$ for alumina (Al_2O_3).

ξ	α	ϕ	$-C_{fx}Re^{1/2}$	$Nu_xRe^{1/2}$
0.5 (Crest)		0.0	1.1175	1.0575
	0.1	0.1	1.1243	1.0415
	0.0		0.87458	0.90201
	0.05	0.2	1.0014	0.9503
			1.1440	0.9914
1.0 (Node)	01	0.0	0.9856	1.4446
		0.1	0.89303	1.4385
	0.0		0.52946	1.2823
	0.05	0.2	0.60696	1.3505
	0.1		0.69547	1.4188
1.5 (Trough)		0.0	0.95052	1.7091
	0.1	0.1	0.96164	1.6845
	0.0		0.75731	1.4777
	0.05	0.2	0.86805	1.5482
	0.1		0.99431	1.6182

Table 6: Percent increase in skin friction and Nusselt number for alumina (Al_2O_3) in comparison to pure fluid ($\phi = 0$) and flat plate case $\alpha = 0$ when Pr = 7.0, $M = 0.5$.

ξ	α	ϕ	% increase in $-C_f$	% increase in Nu
0.5 (Crest)	0.0		30.9	10.6
	0.1	0.1	30.9	10.9
		0.0	0.0	0.0
	0.2	0.05	14.5	5.4
			30.8	10.8
1.0 (Node)	0.0	0.1	31.3	10.3
	0.1		31.3	10.4
		0.0	0.0	0.0
	0.2	0.05	14.6	5.3
			31.4	10.6
1.5 (Trough)	0.0	0.1	31.5	9.5
	0.1		31.4	9.5
		0.0	0.0	0.0
	0.2	0.05	14.6	4.8
		0.1	31.3	9.5

friction and Nusselt number for different nanoparticles (MWCNT, SWCNT, Al_2O_3, TiO_2, Ag) when Pr = 7.0, $M = 0.5$, $\alpha = 0.2$, $\phi = 0.1$, in comparison to pure flat and wavy plate. It is observed that the maximum increase of about 47.3 % in skin friction is obtained for Ag with 10 % concentration in the base fluid and minimum increase of about 27.2 % in the value of skin friction is obtained for SWCNT with 10 % concentration when the present results are compared with the value $f''(0.5, 0) = 0.87458$ at $\alpha = 0.2$ and $\phi = 0.0$. On the other hand, maximum gain of 10.8 % in Nusselt number is obtained for Al_2O_3 and minimum of 8.1 % for Ag with 10 % concentration in the base fluid when the present results are compared with Nu = 0.90201 at $\alpha = 0.2$ and $\phi = 0.0$. The percent increase in skin friction and Nusselt number is also calculated in comparison to $f''(0) = 0.8539$ and Nu = 0.9531 at $\alpha = 0.0$ and $\phi = 0.0$. A maximum of 50.8 % and 4.8 % increase in skin friction and Nusselt number is obtained and a minimum of 27.6 % and 2.3 % increase in skin friction and Nusselt number is obtained, respectively. Through this table, it is easy to identify the role of surface roughness and nanofluid toward heat transfer enhancement. This study reveals that Al_2O_3 nanoparticle has the capacity to produce a coolant (nanofluid) with higher rate of heat transfer.

5 Conclusion

Heat transfer enhancement due to nanofluid and surface texture of the moving rough plate has been computed. Governing non-similar equations have been solved numerically. The accuracy and validity of numerical procedure is ensured by comparing with the results already present in literature. It is observed that the velocity and temperature grow within the boundary layer by increasing the parameter α. Consequently, the skin friction and Nusselt number decrease by increasing the values of α. It is noted that the skin friction increases by increasing the solid

Table 7: Percent change in skin friction and Nusselt number for different nanoparticle when $M = 0.0$, Pr = 7.0, $\alpha = 0.2$, $\phi = 0.1$.

ξ	Nanoparticle material	% increase in $-C_f$		% increase in Nu	
		Verses $f''(0) = 0.8539$ at $\alpha = \phi = 0.0$	Verses $f''(0.5, 0) = 0.87458$ at $\alpha = 0.2, \phi = 0.0$	Verses Nu = 0.9531 at $\alpha = \phi = 0.0$	Verses Nu = 0.90201 at $\alpha = 0.2, \phi = 0.0$
0.5	Al_2O_3	34.0	30.8	4.8	10.8
	Ag	50.8	47.3	2.3	8.1
	TiO_2	34.7	31.5	2.9	8.7
	SWCNT	30.3	27.2	2.9	8.7
	MWCNT	27.6	24.6	3.5	9.4

volume fraction of nanoparticle. Similar trend of Nusselt number is noted for increasing values of ϕ; this observation highlights the fact that by increasing the nanoparticle concentration, the momentum and thermal transport are also enhanced and provides the reason for recommending the nanofluid as a preferred coolant. Nanoparticle of five different metals is used and percent increase in the rate of heat transfer is calculated. Maximum gain of about 10.8 % is obtained for Al_2O_3 nanoparticle with 10 % concentration and minimum of 8.1 % increase is noted for Ag with 10 % concentration in the nanofluid. Our study reveals that the alumina (Al_2O_3) forms good coolant in comparison to the other four metals.

Nomenclature

c_p	Specific heat
g	Acceleration of gravity
κ	Thermal conductivity
l	Characteristic length of the wavy plate
M	Magnetic number
$\bar{p}$	Dimensional pressure
p	Dimensionless pressure
Pr	Prandtl number
S	Wavy surface
T	Local temperature
$(\bar{u}, \bar{v})$	Velocity component in $(\bar{x}, \bar{y})$ direction
(u, v)	Velocity component in (x, y) direction
$(\bar{x}, \bar{y})$	Dimensional coordinates
(x, y)	Dimensionless coordinates

Greek symbols

α	Amplitude of the wavy surface
α^*	Thermal diffusivity
β	Coefficient of thermal expansion
θ	Dimensionless temperature
ϕ	Solid volume friction
μ	Dynamic viscosity
ρ	Local density
(ξ, η)	New computational independent variables
ν	Kinematic viscosity
σ	Electrical conductivity
ψ	Dimensionless stream function

Subscript

f	Base fluid
nf	Nanofluid
p	Nanoparticle
w	Condition at the surface
∞	Condition far away from surface

References

[1] S. U. S. Choi, FED **231**, 99 (1995).
[2] S. U. S. Choi, Z. G. Zhang, W. Yu, F. E. Lockwood, and E. A. Grulke, App. Phys. Lett. **79**(14), 2252 (2001).
[3] Y. Ding, H. Chen, L. Wang, C. Y. Yang, Y. He, et al., KONA, **25**, 23 (2007).
[4] J. Buongiorno, J. Heat Transf. **128**, 240 (2006).
[5] J. Buongiorno and W. Hu, Proc. Int. Conf. Advan. Petrochem. Polym. (ICAPP 05), Seoul, (2005) 5705.
[6] R. K. Tiwari and M. K. Das, Int. J. Heat Mass Transf. **50**, 2002 (2007).
[7] D. A. Nield and A. V. Kuznetsov, Int. J. Heat Mass Transf. **52**, 5792 (2009).
[8] A. V. Kuznetsov and D. A. Nield, Int. J. Therm. Sci. **49**, 243 (2010).
[9] A. V. Kuznetsov and D. A. Nield, Int. J. Heat Mass Trans. **54**, 374 (2011).
[10] A. J. Chamkha and S. E. Ahmed, Chem. Eng. Commu. **199**, 122 (2012).
[11] A. J. Chamkha and S. E. Ahmed, Unsteady MHD heat and mass transfer by mixed convection flow in the forward stagnation region of a rotating sphere in the presence of chemical reaction and heat source. Proceedings of the World Congress on Engineering. 1 (2011).
[12] N. S. Bondareva, M. A. Sheremet, and I. Pop, Int. J. Numer. Meth. Heat Fluid Flow **25**, 1924 (2015).
[13] A. Mahdy and S. E. Ahmed, Eng. Sci. Technol. **18**, 24 (2015).
[14] B. C. Sakiadis, AIChE J. **7**, 26 (1961).
[15] B. C. Sakiadis, AIChE J. **7**, 221 (1961).
[16] N. Bachok, A. Ishak, and I. Pop, Int. J. Therm. Sci. **49**, 1663 (2010).
[17] S. Ahmad, A. M. Rohni, and I. Pop, Acta Mech. **218**, 195 (2011).
[18] N. Dalir and S. S. Nourazar, Mechanika **20**, 57 (2014).
[19] O. D. Makinde, Appl. Math. Mech. **33**, 1545 (2012).
[20] E. Abu-Nada, Int. J. Heat Fluid Flow **29**, 242 (2008).
[21] H. F. Oztop and E. Abu-Nada, Int. J. Heat Fluid Flow **29**, 1326 (2008).
[22] E. Abu-Nada and H. F. Oztop, Int. J. Heat Fluid Flow **30**, 669 (2009).
[23] N. Bachok, A. Ishak, and I. Pop, Int. J. Heat Mass Transf., **55**, 642 (2012).
[24] N. Bachok, A. Ishak, and I. Pop, Acta Mech. Sin. **28**, 34 (2012).
[25] I. Mustafa, T. Javed, and A. Majeed, Canad. J. Phys. **93**, 1365 (2015).
[26] D. A. S. Rees and I. Pop, Fluid Dyn. Res. **14**, 151 (1994).
[27] D. A. S. Rees and I. Pop, Acta Mech. **112**, 149 (1995).
[28] M. A. Hossain and I. Pop, Acta Mech. **48**, 813 (1996).
[29] S. E. Ahmed and M. A. El-Aziz, Meccanica **48**, 33 (2013).
[30] R. S. R. Gorla and M. Kumari, J. Nano Eng. Nano Sys. **225**, 133 (2011).
[31] M. Narayana, P. Sibanda, S. S. Motsa, and P. G. Siddheshwar, Boundr. Val. Probl. **88**, 1 (2012).
[32] M. A. Sheremet and I. Pop, J. Heat Transf. **137**, 072601 (2015).
[33] A. Ghaffri, T. Javed, and F. Labropuluo, J. Therm. Sci. (2015), DOI: 10.2298/TSCI150411163G.
[34] M. A. Sheremet, I. Pop, and N. Bachok, Int. J. Heat Mass Transf. **92**, 1053 (2016).

[35] M. A. Sheremet, I. Pop, and A. Shenoy, Int. Commun. Heat Mass Transf. **67**, 66 (2015).
[36] T. Javed, Z. Mehmood, A. M. Siddique, and I. Pop, Int. J. Num. Meh. Heat Fliud Flow (2016), DOI 10.1108/HFF-10-2015-0448.
[37] H. M. Elshehabey, F. M. Hady, S. E. Ahmed, and R. A. Mohamed, Int. Commun. Heat Mass Transf. **57**, 228 (2014).
[38] J. C. Maxwell Garnett, Philos. Trans. R. Soc. Lond. A **203**, 385 (1904).
[39] S. E. Ahmed and A. Mahdy, App. Math. Mech. Engl. Ed., **37**, 471 (2016).
[40] A. Mahdy and S. E. Ahmed, Transp. Porous Med. **91**, 423 (2012).
[41] T. Cebeci and P. Bradshaw, Physical and Computational Aspects of Convective Heat Transfer, Springer, New York 1988.
[42] T. Cebeci and P. Bradshaw, Momentum Transfer in Boundary Layers, Hemisphere, Washington 1977.
[43] T. Cebeci, K. C. Chang, and P. Bradshaw, Comp. Meth. Appl. Mech. Eng. **22**, 213 (1980).
[44] T. Y. Na, Computational Methods in Engineering Boundary Value Problems, Academic Press, New York 1979.
[45] T. C. Chiam, Acta Mech., **122**, 169 (1997).